Neutron inelastic scattering from ^{54,56}Fe

S. Mellema* and R. W. Finlay
Department of Physics, Ohio University, Athens, Ohio 45701

F. S. Dietrich
Lawrence Livermore National Laboratory, Livermore, California 94550
(Received 22 July 1985)

Differential cross sections for inelastic scattering of neutrons to numerous levels in ^{54,56}Fe have been measured at incident neutron energies of 11 and 26 MeV. The data have been analyzed in terms of a collective model using a distorted-wave Born approximation as well as a full coupled-channels treatment. Analysis has also been performed with a microscopic folding model using an energy- and density-dependent effective interaction. Both collective and microscopic analyses have also been applied to inelastic proton scattering in the same energy region in order to extract information on the isospin nature of the measured excitations.

I. INTRODUCTION

Nucleon inelastic scattering is potentially a very powerful probe of nuclear structure. At sufficiently high incident energies, strongly collective states are preferentially excited. The isospin composition of these excitations may be investigated through a comparison of proton and neutron inelastic scattering. One topic of special interest in this regard has been the identification of isovector deformations which occur at or near the shell closures, in particular for the first 2^+ excited states in singly-closed-shell nuclei. The core polarization models of Brown, Madsen, and collaborators[1-3] have provided a formulation for understanding these effects, and detailed experimental results have been published for the shell closures $N=50$ (Ref. 4) and $Z=50$ (Ref. 5).

The aim of the present work is to study these effects for ^{54,56}Fe, and in particular to investigate whether or not the observed isovector effects at shell closure (^{54}Fe, $N=28$) are appreciably changed by adding a single pair of neutrons outside the closed shell (^{56}Fe), and whether or not these effects are observed in higher excited states including states of higher multipolarity (e.g., $L=3$).

As is the case for many nuclei, inelastic proton scattering measurements resolving low-lying states in ^{54,56}Fe have been carried out since the late 1960's,[6-10] whereas neutron scattering measurements have been limited by resolution and background difficulties to elastic scattering, or at best have included inelastic scattering to the first excited states which are well separated in energy from the ground state.[11-13] However, the Ohio University beam swinger time-of-flight (TOF) facility[14] with its extremely low background, high count rate, and excellent resolution ($\Delta E/E \sim 1$–2%) permits the practical measurement of inelastic neutron scattering cross sections to states previously observed only with charged particles. The number of states for which the isospin may be studied is thus greatly increased.

In the present work, differential cross sections for a number of low-lying states in both ^{54,56}Fe have been measured at incident energies of 11 and 26 MeV. At 11 MeV eight inelastic levels have been measured for ^{54}Fe, while eleven have been measured for ^{56}Fe. At 26 MeV, six inelastic states have been measured for ^{54}Fe, while only two states were strongly excited in ^{56}Fe.

The analysis of the present data and the comparison to available proton scattering data has been carried out in three steps. First, a standard collective model distorted-wave Born approximation (DWBA) analysis has been performed using optical model potentials derived from a previous analysis of elastic scattering at these energies. Second, a full coupled-channels analysis has been performed including all states observed to be strongly excited by direct reaction. Finally, a microscopic folding-model analysis has been carried out using a density-dependent effective interaction derived from nuclear matter calculations in order to calculate scattering in the DWBA.

II. EXPERIMENTAL TECHNIQUES

The measurements were made using the Ohio University Tandem Van de Graaff accelerator and beam swinger TOF spectrometer, which has been described in detail elsewhere.[14] Details of the specific neutron sources, scattering samples, and neutron detectors used are given in Ref. 15, which describes the analysis of elastic scattering data from the same isotopes. In summary, a pulsed and bunched deuteron beam was incident upon a deuterium (tritium) gas target producing 11 MeV (26 MeV) neutrons via the ^{2}H(d,n)^{3}He [^{3}H(d,n)^{4}He] reaction. Separated isotope samples of ^{54,56}Fe were placed ~ 14 cm from the neutron source, and the scattered neutrons were observed in a sevenfold array of liquid scintillator detectors at a flight path of 13 m. Neutron–gamma-ray pulse-shape discrimination was used, and a monitor detector, placed at a fixed angle relative to the zero degree line, observed the direct flux of neutrons from the gas target.

The effective energy resolution in the TOF measurements was sufficient to resolve a number of low-lying levels in both nuclei. The resolution at 11 MeV was ~ 200

keV full width at half maximum (FWHM) and ~430 keV FWHM at 26 MeV. Measurements were taken both with the scattering sample present and with the sample removed in order to subtract background. Figure 1 shows typical sample-in and sample-out spectra for ^{56}Fe(n,n') at 11 MeV. As can be seen, the signal to noise ratio is very good due to the excellent shielding and collimation provided by the beam swinger facility, with the only important contribution to the sample-out spectrum coming from the ever-present elastic scattering of neutrons from air surrounding the sample.

Figure 2 shows a typical background-subtracted spectrum for ^{54}Fe(n,n') at 26 MeV. The yields under the various inelastic peaks have been extracted using a least-squares peak fitting program which allows skewed shaping to account for both multiple scattering and for the low-energy tails which are typical of the large-volume scintillation detectors.

Table I summarizes the states for which differential cross sections were extracted. In cases where the experimental resolution was insufficient to distinguish known nuclear levels, a comparison was made with previously published proton scattering measurements in order to determine which levels were excited.

To normalize the relative cross sections thus obtained, the main detectors were placed at 0° in order to measure the flux per monitor count which would have been incident upon the scattering sample. The data were then corrected for the anisotropy of the neutron source reaction and for the relative efficiency of the neutron detectors,

$$\{\text{efficiency}[E_R(0°)]/\text{efficiency}[E_R(\theta)]\}\ ,$$

which was measured in an independent experiment. While the source anisotropy correction was on the order of 2–3%, the relative efficiency correction for neutrons scattered inelastically to energies well below that of the incident beam was as much as 40%.

Finally, the cross sections were corrected for flux at-

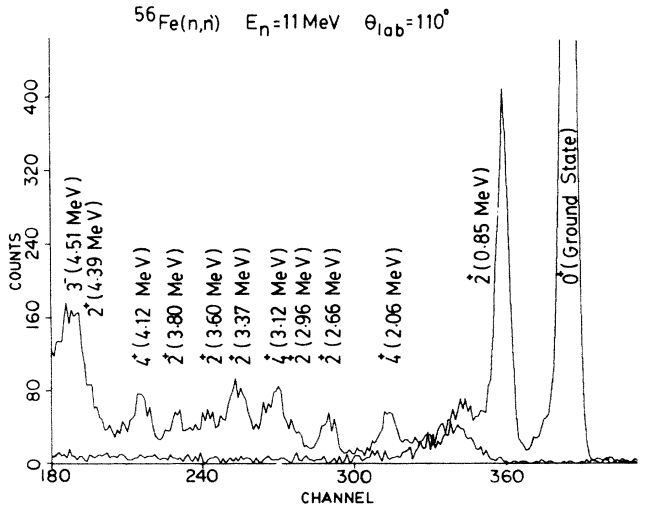

FIG. 1. Sample-in and sample-out time-of-flight spectra for ^{56}Fe(n,n') at 11 MeV at a lab angle of 110°.

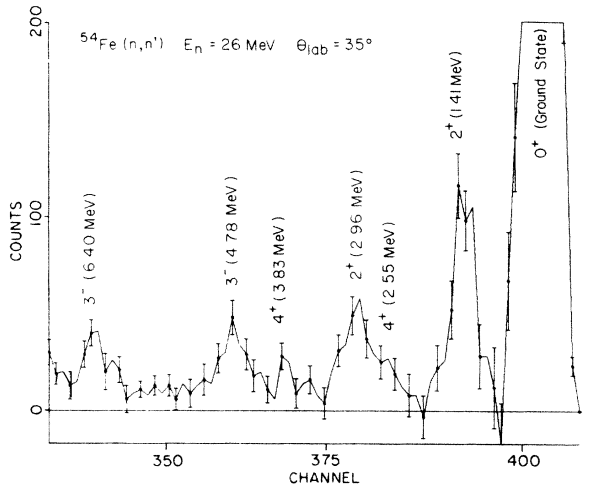

FIG. 2. Background subtracted time-of-flight spectrum for ^{54}Fe(n,n') at 26 MeV at a lab angle of 35°.

TABLE I. Inelastic levels for which differential cross sections were measured in the present work. An asterisk indicates spin and parity assigned to the same state observed in (p,p'), even though in the present measurement the state was not resolvable from what are assumed to be very weakly excited neighboring states.

Nucleus	Excitation energy (MeV)	J^π	$d\sigma/d\Omega$ measured at E_n (MeV)
^{54}Fe	1.41	2^+	11, 26
	2.54*	4^+	11, 26
	2.96*	2^+	11, 26
	3.17	2^+	11
	3.30*	4^+	11
	3.83	4^+	11, 26
	4.05*	4^+	11
	4.27*	4^+	11
	4.78*	3^-	26
	6.40*	3^-	26
^{56}Fe	0.85	2^+	11, 26
	2.09	4^+	11
	2.66	2^+	11
	2.96*	2^+	11
	3.12*	4^+	11
	3.37*	2^+	11
	3.60*	2^+	11
	3.83*	2^+	11
	4.12*	4^+	11
	4.40*	2^+	11
	4.51*	3^-	11, 26

TABLE II. Best fit optical model parameters from elastic scattering analysis. (In all cases $V_{SO}=6.2$, $r_{SO}=1.09$, $a_{SO}=0.75$.)

Nucleus	E_n	V_R	r_R	a_R	W_V	W_D	r_I	a_I
^{54}Fe	11	49.92	1.19	0.633	0.0	7.48	1.25	0.608
	26	44.05	1.19	0.638	2.0	5.50	1.23	0.668
^{56}Fe	11	48.56	1.19	0.660	0.0	7.44	1.25	0.609
	26	44.03	1.19	0.653	0.16	7.18	1.13	0.735

tenuation in the sample, for finite angular geometry, and for multiple scattering using the Monte Carlo code MULCAT.[16] The final data reflect uncertainties due primarily to counting statistics enhanced by the uncertainty of the peak fitting procedure. Typical errors range from less than 10% for strongly excited inelastic states to as much as 30% for very weakly excited states. However, the overall normalization of the data is known to $<3\%$ due to the small uncertainties in the 0° flux and the detector relative efficiency.

TABLE III. Calculated compound nuclear contributions to scattering states at 11 MeV are compared with the measured cross sections.

Nucleus	State	Measured cross section (mb)	CN calculation (mb)
^{54}Fe	g.s.	1467.39	0.98
	2_1^+ (1.41 MeV)	42.03	3.62
	4_1^+ (2.55 MeV)	7.66	4.20
	2_2^+ (2.96 MeV)	17.07	3.24
	2_3^+ (3.17 MeV)	9.31	3.19
	4_2^+ (3.30 MeV)	8.00	3.75
	4_3^+ (3.83 MeV)	6.82	3.77
	4_4^+ (4.05 MeV)	7.81	3.69
	4_5^+ (4.27 MeV)	7.59	3.62
^{56}Fe	g.s.	1478.81	0.74
	2_1^+ (0.85 MeV)	82.53	2.82
	4_1^+ (2.09 MeV)	5.71	3.27
	2_2^+ (2.66 MeV)	7.30	2.48
	2_3^+ (2.96 MeV)	4.80	2.42
	4_2^+ (3.12 MeV)	10.63	3.02
	2_4^+ (3.37 MeV)	12.46	2.35
	2_5^+ (3.60 MeV)	6.44	2.30
	2_6^+ (3.83 MeV)	5.47	2.26
	4_3^+ (4.12 MeV)	7.66	2.76
	2_7^+ (4.40 MeV)	6.37	2.14
	3_1^- (4.51 MeV)	22.90	2.65

III. REACTION-MODEL ANALYSIS

A. Spherical optical model

The starting point of the analysis is the optical model potential used to describe the elastic scattering data. Both conventional phenomenological as well as microscopic optical-model analyses of elastic scattering from these isotopes at 20, 22, 24, and 26 MeV have been presented in Ref. 15. The results of a best-fit phenomenological optical model search on the 11 MeV data are shown in Fig. 3. A tabulation of the best-fit optical model potential parameters for elastic scattering from both isotopes at 11 and 26 MeV is given in Table II.

As a check on the accuracy of the overall normalization of the measurements, the graph of ^{56}Fe(n,n) also includes

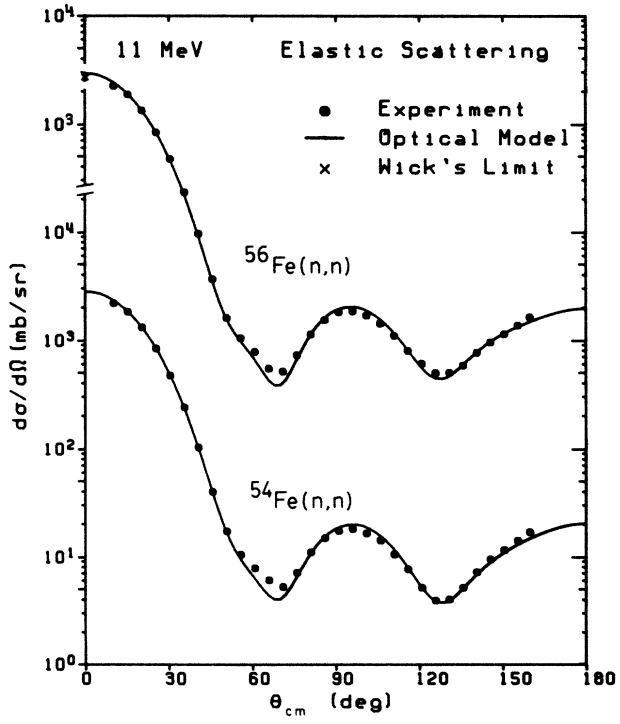

FIG. 3. Differential cross sections for elastic scattering of 11 MeV neutrons from ^{54,56}Fe are compared to best-fit phenomenological optical model calculations. The value of Wick's limit is calculated from the total cross section of Ref. 17.

a point for $d\sigma/d\Omega(0°)$ calculated according to Wick's limit based upon the value for the total cross section of ^{nat}Fe from a recent compilation.[17] It is noteworthy that a Legendre polynomial fit through the differential cross section data not including the point at 0° (not shown) agrees with Wick's limit at 0° to within 2%. This agreement also holds true at 26 MeV, and gives confidence in the overall normalization of all the cross section data.

B. Compound nuclear contributions

The plethora of weakly excited states which were measured at 11 MeV is due not only to improved resolution at that energy, but also to the contribution of compound nuclear (CN) reactions to the cross sections. Since the purpose of the present work is to analyze these excitations in terms of direct reaction theories, it is necessary first to calculate the CN contributions to each inelastic state.

These calculations were performed using the Hauser-Feshbach model including Porter-Thomas width-fluctuation corrections in the computer code HELENE.[18] Open channels included all discrete levels of known spin and parity as well as continuum levels for the (n,n'), (n,p), and (n,α) reactions. The energies, spins, and parities of the discrete levels as well as the level density parameters for the continua were taken from a recent evaluation of neutron-induced reactions on ^{54,56}Fe.[17]

Calculated CN contributions to the measured excitation in the 11 MeV experiment ranged from less than 0.1% for elastic scattering to more than 50% of some of the weakly excited states. A summary of the calculated (integrated) cross sections is given in Table III.

The procedure for analyzing the 11 MeV data was, therefore, to subtract the CN contribution from the measured differential cross section data and then to analyze the difference in terms of direct reaction theory. Finally, the sum of the CN and direct reaction calculations is compared to the actual experimental data.

CN contributions at 26 MeV are negligible.

C. DWBA analysis

The inelastic cross sections were analyzed in the distorted-wave Born approximation using a vibrational model with complex form factors, viz.,

$$F=\beta_L R\frac{dU}{dr}Y_{L0}(\theta)\ , \tag{1}$$

where U is the optical potential from the elastic scattering analysis and L is the angular momentum transfer to the state of interest. The transition amplitudes were calculated in the computer code DWUCK4 (Ref. 19) as

$$T_{fi}=\left\langle \chi_f^{(-)}\left|\frac{F}{\beta_L}\right|\chi_i^{(+)}\right\rangle\ , \tag{2}$$

where the χ's are the (distorted) wave functions in the entrance and exit channels calculated from the optical potentials (with the exit-channel potential adjusted for the ejectile energy appropriate to that channel).

The values of β_L were determined by renormalizing the calculated DWBA cross sections for best agreement with the experimental data. The results of the calculations are shown in Figs. 4—7.

In general the agreement between the data and calculations is quite reasonable. However, there is an anomaly in the results for the first 2^+ states for both ^{54,56}Fe at 26 MeV. The sharp rise in the measured cross sections at forward angles ($\theta<25°$) is uncharacteristic of an $L=2$ angular distribution. This will be discussed further in Sec. V.

Table IV contains a summary of the deformation parameters obtained in the DWBA analysis. Notably, for every state (in both nuclei) which was measured at both 11 and 26 MeV, the value of $\beta_{nn'}$ obtained at 11 MeV is lower than the value obtained at 26 MeV. A possible explanation is that the Hauser-Feshbach calculations have overestimated the CN contributions to the inelastic cross sections at 11 MeV.

D. Coupled-channels analysis

Because of the uncertainty in the magnitude of the direct component of the excitations at 11 MeV, a full coupled-channel (CC) analysis was only performed on the 26 MeV data. However, since the aim of a coupled-channels analysis is to include all states whose couplings with the ground state are strong, it seems adequate to include only those states which were observed to be excited at 26 MeV.

Because of its energy level structure, ^{54}Fe has been considered a vibrational nucleus. In the simplest picture, the first 2^+ state (2_1^+, $E_x=1.41$ MeV) is a one-quadrupole-phonon excitation and the 4_1^+ (2.54 MeV), 0_2^+ (2.56 MeV), and 2_2^+ (2.96 MeV) states are two-quadrupole-phonon excitations. However, if such a harmonic vibrational model is applied to ^{54}Fe(n,n') at 26 MeV, the magnitudes of the 4_1^+ and 2_2^+ cross sections are grossly underpredicted.

If one wishes to remain within the framework of a vibrational model, this indicates the presence of anharmonicity in the quadrupole excitations, and the need for a hexadecapole-phonon component in the 4_1^+ state. The presence of a second 4^+ state (4_2^+, 3.83 MeV) may be accommodated as the combination of one-hexadecapole and two-quadrupole phonon configurations that is orthogonal to the 4_1^+ state. Finally, the existence of two strongly excited 3^- states (3_1^-, 4.78 MeV and 3_2^-, 6.40 MeV) may be most simply explained by assuming that these are orthogonal linear combinations of one-phonon (octupole) and two-phonon (quadrupole-octupole) excitations.

Thus the vibrational-model analysis of ^{54}Fe(n,n') involves the coupling of 0_1^+-2_1^+-4_1^+-2_2^+-4_2^+-3_1^--3_2^- in which each of the excited states is an orthogonal combination of one- and two-phonon excitations, and includes quadrupole, octupole, and hexadecapole deformations. The calculations were performed using the code ECIS79.[20] Aside from the optical-potential parameters, this simple model contains six parameters which were adjusted to fit the data; they are the three deformation parameters β_2, β_3, and β_4 and the mixing coefficients for the states of each of the three spins. The analysis began from the optical

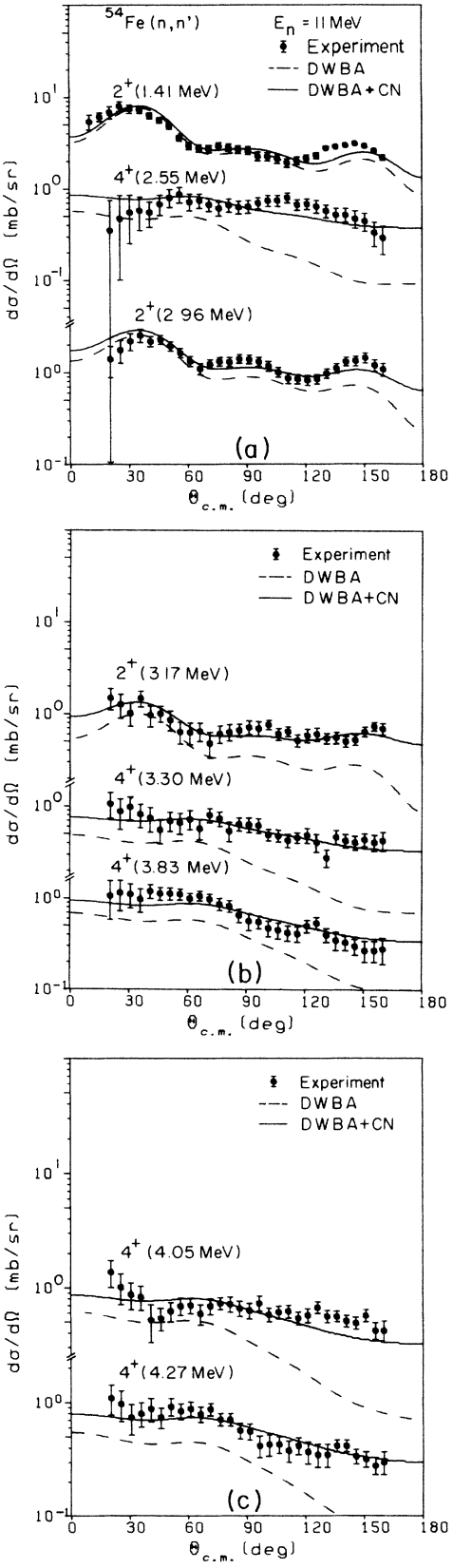

FIG. 4. Differential cross sections for inelastic scattering of 11 MeV neutrons from ^{54}Fe are compared with DWBA calculations. Dashed lines show the calculations of the direct component only; solid lines are the sum of direct and compound nuclear contributions.

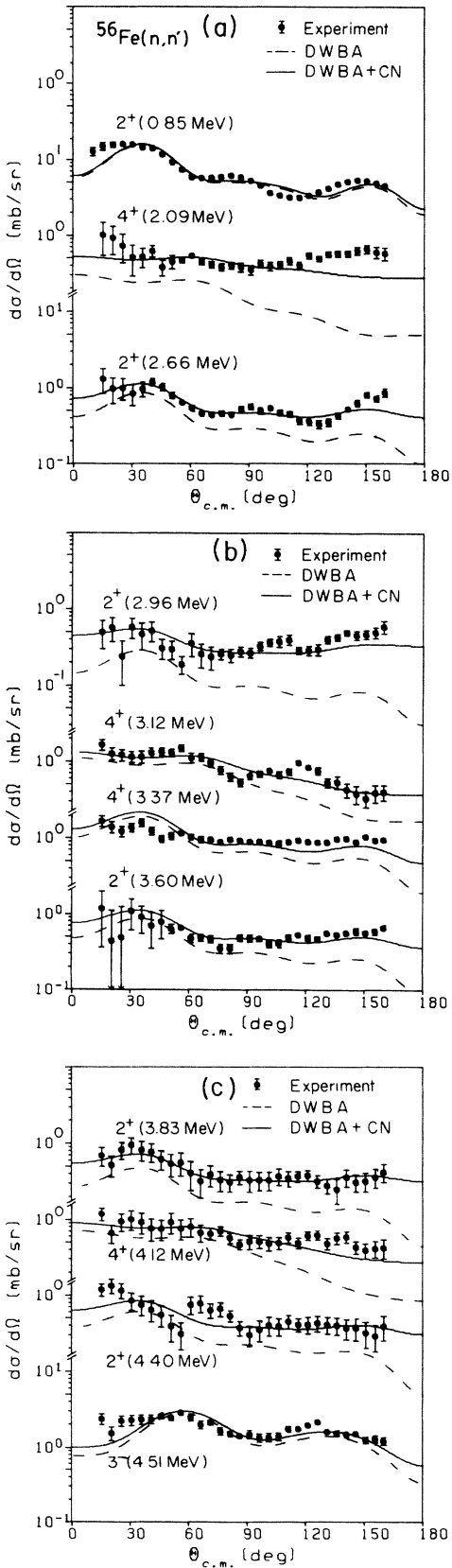

FIG. 5. Differential cross sections for inelastic scattering of 11 MeV neutrons from ^{56}Fe are compared with DWBA calculations. Dashed lines show the calculations of the direct component only; solid lines are the sum of direct and compound nuclear contributions.

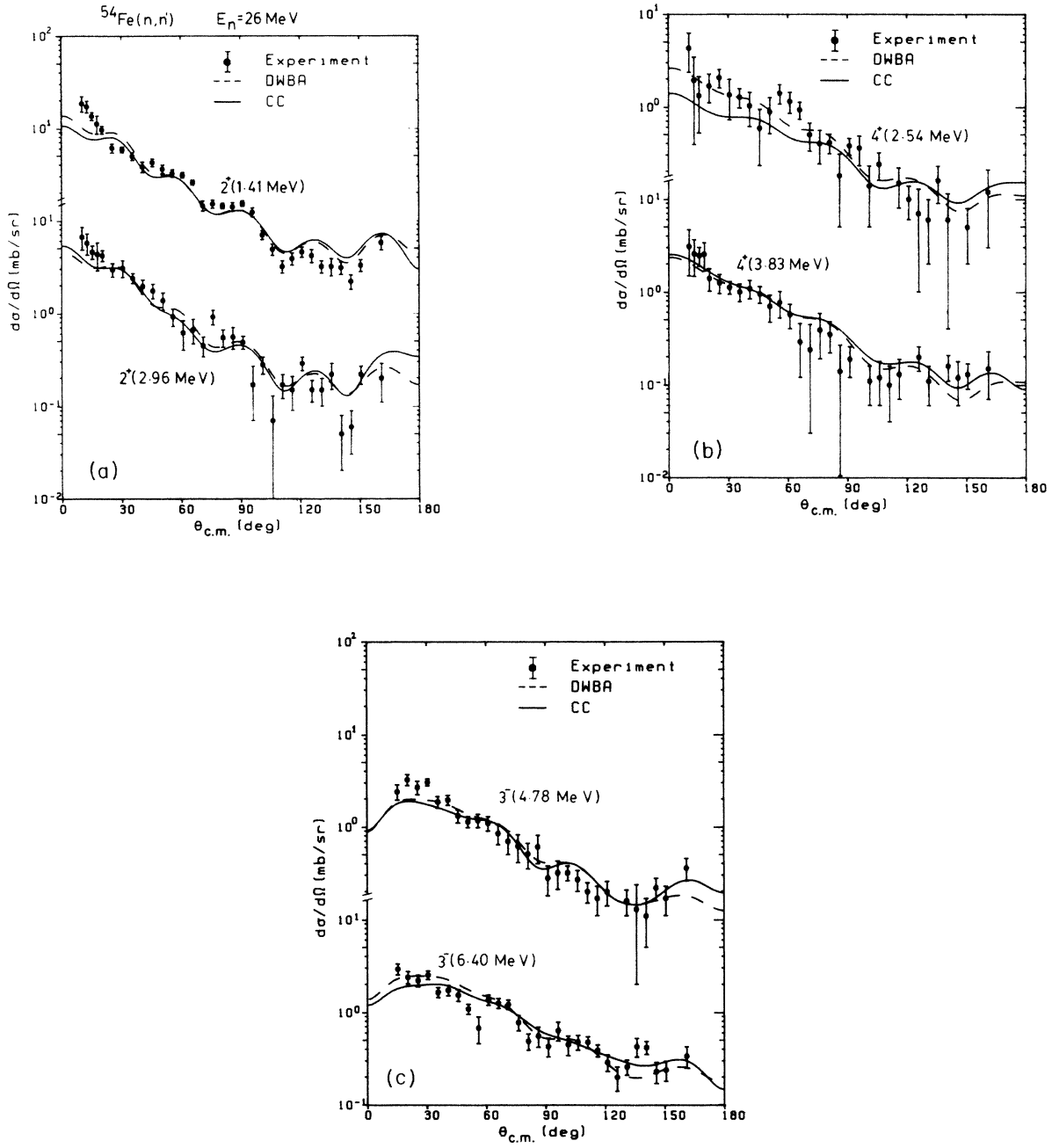

FIG. 6. Differential cross sections for inelastic scattering of 26 MeV neutrons from ^{54}Fe are compared with DWBA calculations (dashed lines) and coupled-channels calculations (solid lines) for (a) the 2^+ states, (b) the 4^+ states, and (c) the 3^- states.

potential of Table II, but the values of V_R and W_D were varied to ensure a fit to the elastic scattering data in the coupled-channels calculation. For the results shown here, $V_R=44.24$ MeV and $W_D=4.55$ MeV were used. The results of the calculations compare quite favorably with the data and are shown in Fig. 6. A summary of the deformation parameters and descriptions of the wave functions of the excited states in terms of one- and two-phonon components is given in Table V.

The structure of low-lying states in ^{56}Fe characterizes it as a deformed or rotational nucleus.[21,22] The recent measurement of a static quadrupole moment for the first 2^+ state (2_1^+, $E_x=0.85$ MeV) supports this model.[23]

However, the present measurement of the strongly excited 3^- state (3_1^-, 4.51 MeV) cannot be described in a purely rotational model. The coupled-channels analysis of ^{56}Fe therefore involves a rotation-vibration model in which the 3^- state is described as the octupole vibration

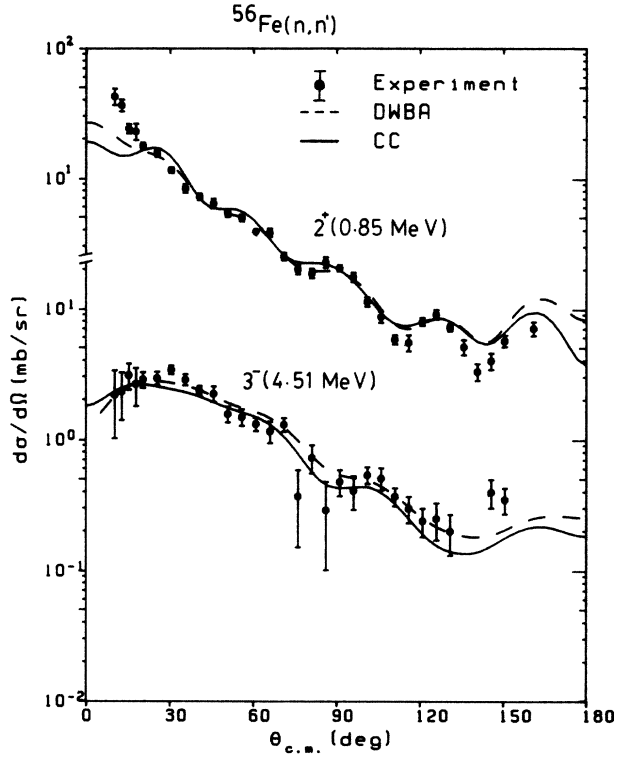

FIG. 7. Differential cross sections for inelastic scattering of 26 MeV neutrons from ^{56}Fe are compared with DWBA calculations (dashed lines) and coupled-channels calculations (solid lines).

of a quadrupole-deformed nucleus.[24] Starting with the optical potential of Table II, the values of V_R and W_D were varied for an optimum fit to the elastic scattering data. The value of β_2 was varied for an optimum fit to the 2_1^+ state, and the magnitude of the reduced matrix element between the ground state and the 3_1^- state was varied for an optimum fit to that state. The results of the calculations are shown as the solid line in Fig. 7. The final values of the adjusted parameters are $V_R=43.82$ MeV, $W_D=6.59$ MeV, $\beta_2=0.245$ MeV, and $\beta_3=0.177$.

While the agreement between the calculations and the data is reasonable in all cases, it can also be seen from Figs. 6 and 7 that there is very little difference in the angular distribution shapes predicted by the simpler DWBA calculations and the full coupled-channel results. Furthermore, the data do not show a preference for any of the subtle differences between the two calculations. The magnitude of β_2 for ^{54}Fe is about 10% greater in the CC than in the DWBA calculation, which is of the order of the uncertainties in determining this parameter. For ^{56}Fe, β_2 is 20% greater in CC than in DWBA, but in this case the models employed were different (rotational versus vibrational). We conclude that it is justifiable to study these low-lying excitations in ^{54,56}Fe via the DWBA without the need to resort to the full coupled-channels formalism.

E. Microscopic DWBA calculations

We have recently[25] presented calculations of inelastic scattering cross sections in a microscopic DWBA approach, in which entrance- and exit-channel optical potentials as well as transition form factors are calculated consistently in a folding model using the energy- and density-dependent t matrix of Brieva and Rook.[26,27] The transition density for a particular inelastic transition is calculated in a Tassie model based upon the ground state charge distribution measured in elastic electron scattering, with the proton transition density $\rho_{tr}^{p}(r)$ being normalized to the value of $B(EL)$ measured by Coulomb excitation or inelastic electron scattering. In the simplest hydrodynamic assumption, the neutron transition density may be found from the relation

$$\rho_{tr}^{n}(r)=\frac{N}{Z}\rho_{tr}^{p}(r)\ . \tag{3}$$

Within the context of this model, this is equivalent to saying that the ratio of neutron and proton transition matrix elements $M_n/M_p=N/Z$. Of course, such a relation is only expected to be valid in the absence of strong isovector effects such as those which may be present due to shell closure, e.g., in ^{54}Fe, which is a single-closed-shell nucleus with $N=28$.

In fact, the conclusion of our earlier work is that Eq. (3) is not valid for the 2_1^+ transition in ^{54}Fe. In order to fit consistently both proton and neutron inelastic scattering to this state, the model requires that $M_n/M_p=0.8\pm0.1$.[25] This will be addressed in more detail in Sec. IV. We have now extended the microscopic DWBA analysis testing the assumption of Eq. (3) to the 2_2^+, 3_1^-, and 3_2^- states in ^{54}Fe.

For the 2_2^+ state in ^{54}Fe there are two values in the literature of $B(E2{:}0^+\rightarrow2^+)=225+10$ e^2fm^4 (Ref. 28) and 136 ± 23 e^2fm^4 (Ref. 29). Use of the former value (obtained from inelastic electron scattering) to normalize the proton transition density, along with Eq. (3) to calculate the neutron transition density, led to good agreement with the measurements for this state. The results for (n,n') are compared to the present work in Fig. 8(a) and the results for (p,p') are compared to the data of Van Hall *et al.*[9] at 17.2, 20.4, and 24.6 MeV in Fig. 8(b).

Calculations were also performed for the two 3^- states in ^{54}Fe. Using the assumption of Eq. (3) with the values $B(E3{:}0^+\rightarrow3^-)=6670$ e^2fm^6 and $B(E3{:}0^+\rightarrow3_2^-)=8960$ e^2fm^6, the predicted cross sections are consistent with both the present neutron measurements and with the proton measurements of Eccles *et al.*,[6] as shown in Figs. 9 and 10. The only measured $B(E3)$ values,[10] determined from electron scattering over a limited q^2 range, are 4390 e^2fm^4 for the 3_1^- and 6110 e^2fm^6 for the 3_2^- states; these values are about 30% smaller than those required to fit the nucleon-scattering data.

The microscopic model was also applied to the 2_1^+ and 3_1^- states in ^{56}Fe. The value of $B(E2{:}0^+\rightarrow2_1^+)=1022$ e^2fm^4, obtained in a recent Coulomb excitation measurement, yields reasonable agreement with both neutron and proton scattering data, using Eq. (3) to relate the neutron and proton densities. These results are shown in Fig. 11.

TABLE IV. Deformation parameters obtained from DWBA analysis of the present work. The radius parameter was $r_R = 1.19$ fm.

Nucleus	State	Incident energy (MeV)	$\beta_{nn'}$
^{54}Fe	2_1^+ (1.41 MeV)	11	0.179±0.002
		26	0.193±0.020
	4_1^+ (2.55 MeV)	11	0.079±0.012
		26	0.124±0.020
	2_2^+ (2.96 MeV)	11	0.107±0.010
		26	0.121±0.019
	2_3^+ (3.17 MeV)	11	0.069±0.006
	4_2^+ (3.30 MeV)	11	0.078±0.016
	4_3^+ (3.83 MeV)	11	0.080±0.010
		26	0.122±0.010
	4_4^+ (4.05 MeV)	11	0.097±0.005
	4_5^+ (4.27 MeV)	11	0.078±0.015
	3_1^- (4.78 MeV)	26	0.141±0.009
	3_2^- (6.40 MeV)	26	0.167±0.020
^{56}Fe	2_1^+ (0.85 MeV)	11	0.252±0.018
		26	0.292±0.020
	4_1^+ (2.09 MeV)	11	0.079±0.013
	2_2^+ (2.66 MeV)	11	0.062±0.007
	2_3^+ (2.96 MeV)	11	0.040±0.016
	4_2^+ (3.12 MeV)	11	0.110±0.009
	2_4^+ (3.37 MeV)	11	0.095±0.012
	2_5^+ (3.60 MeV)	11	0.063±0.012
	2_6^+ (3.83 MeV)	11	0.047±0.006
	4_3^+ (4.12 MeV)	11	0.100±0.010
	2_7^+ (4.40 MeV)	11	0.059±0.017
	3_1^- (4.51 MeV)	11	0.200±0.015
		26	0.201±0.020

The two reported measurements of $B(E3{:}0^+ \rightarrow 3^-)$, both from electron scattering, are discrepant (10370 e^2fm^6 from Ref. 28 vs 16600 e^2fm^6 from Ref. 30). The larger of these values is about 30% less than the value of 23200 e^2fm^6 required for a reasonable fit to the magnitude of the neutron and proton scattering data, as shown in Fig. 12; the assumption of Eq. (3) was again employed.

TABLE V. Parameters used in the coupled-channels analysis of ^{54}Fe(n,n') at 26 MeV. The deformation parameters were $\beta_2 = 0.212$, $\beta_3 = 0.185$, and $\beta_4 = 0.139$.

State	One-phonon component	Two-phonon component
2_1^+	−0.500	+0.866
2_2^+	+0.866	+0.500
4_1^+	−0.819	+0.574
4_2^+	+0.574	+0.819
3_1^-	+0.766	+0.643
3_2^-	+0.643	−0.766

The shapes of the angular distributions for the 2^+ and 3^- excitations in both nuclei are rather well reproduced by the calculations. The magnitudes are well predicted for the 2^+ excitations. However, even though there are discrepancies in the $B(E3)$ measurements, the calculations for the 3^- states appear to underestimate the data by about 30%. This result is consistent with the findings in related work[31] that the Brieva-Rook interaction underestimates the cross sections for the lower 3^- states in ^{16}O and ^{208}Pb at low energies (< 30 MeV); in these cases detailed electron-scattering transition densities were available, and the agreement at higher energies (40—60 MeV) was acceptable. In principle, nucleon scattering is sensitive to more details of the shape of the transition density than the $B(EL)$ values, which are a particular radial moment of the density. A goal of the microscopic calculations is to develop a reaction model that is reliable enough to yield this information, and the results for the 2^+ excitations are encouraging. However, the apparent lack of consistency between the two multipolarities in the energy range of the

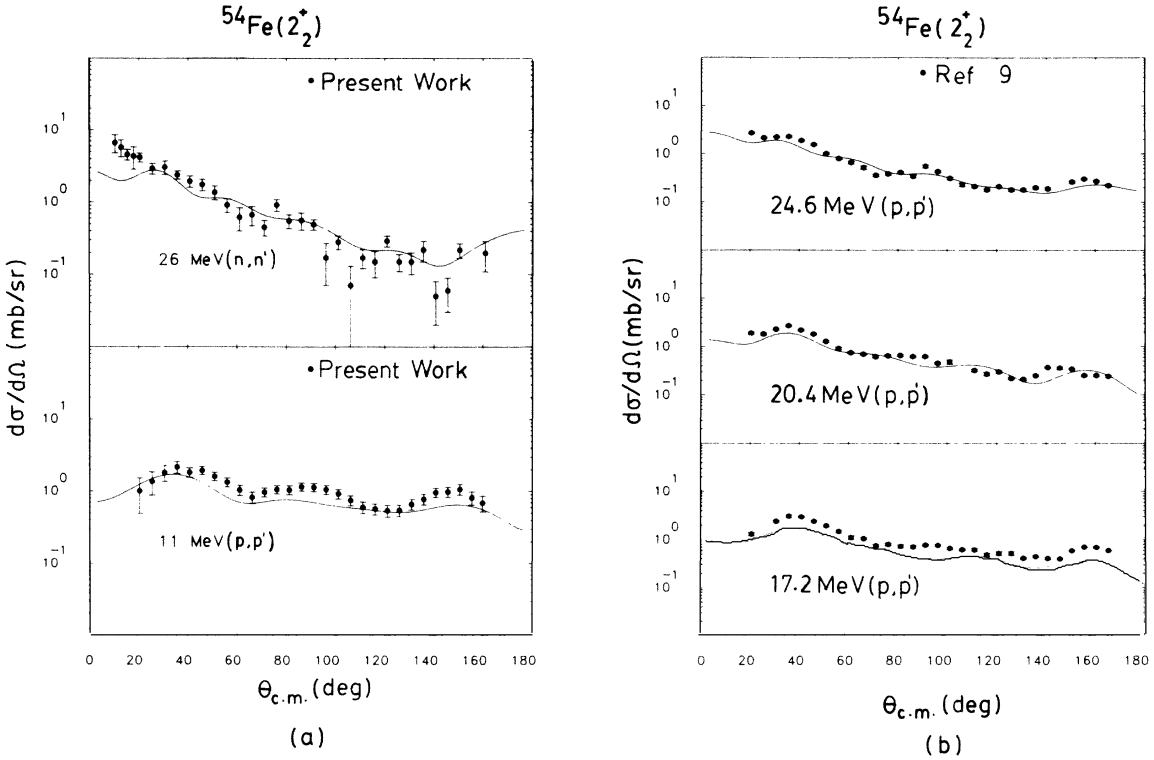

FIG. 8. Microscopic DWBA calculations of scattering to the 2_2^+ state ($E_x = 2.96$ MeV) in ^{54}Fe are compared to (a) the neutron data of the present work and (b) the proton data of Ref. 9.

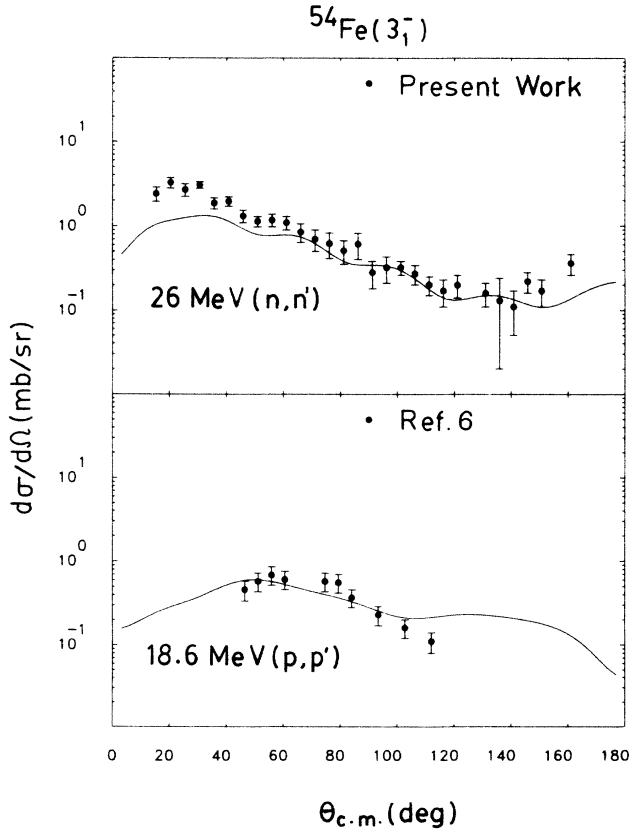

FIG. 9. Microscopic DWBA calculations of scattering to the 3_1^- state ($E_x = 4.78$ MeV) in ^{54}Fe are compared to the neutron data of the present work and the proton data of Ref. 6.

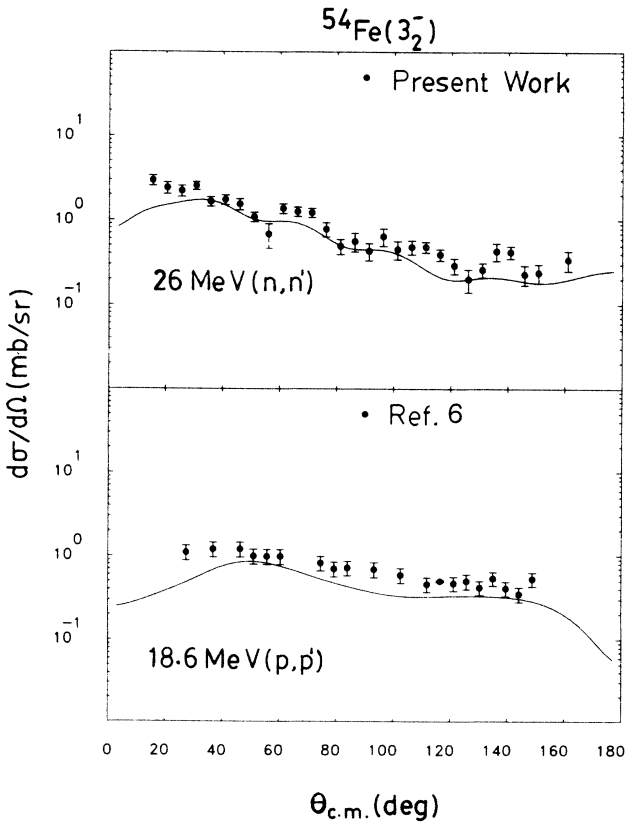

FIG. 10. Microscopic DWBA calculations of scattering to the 3_2^- state ($E_x = 6.40$ MeV) in ^{54}Fe are compared to the neutron data of the present work and the proton data of Ref. 6.

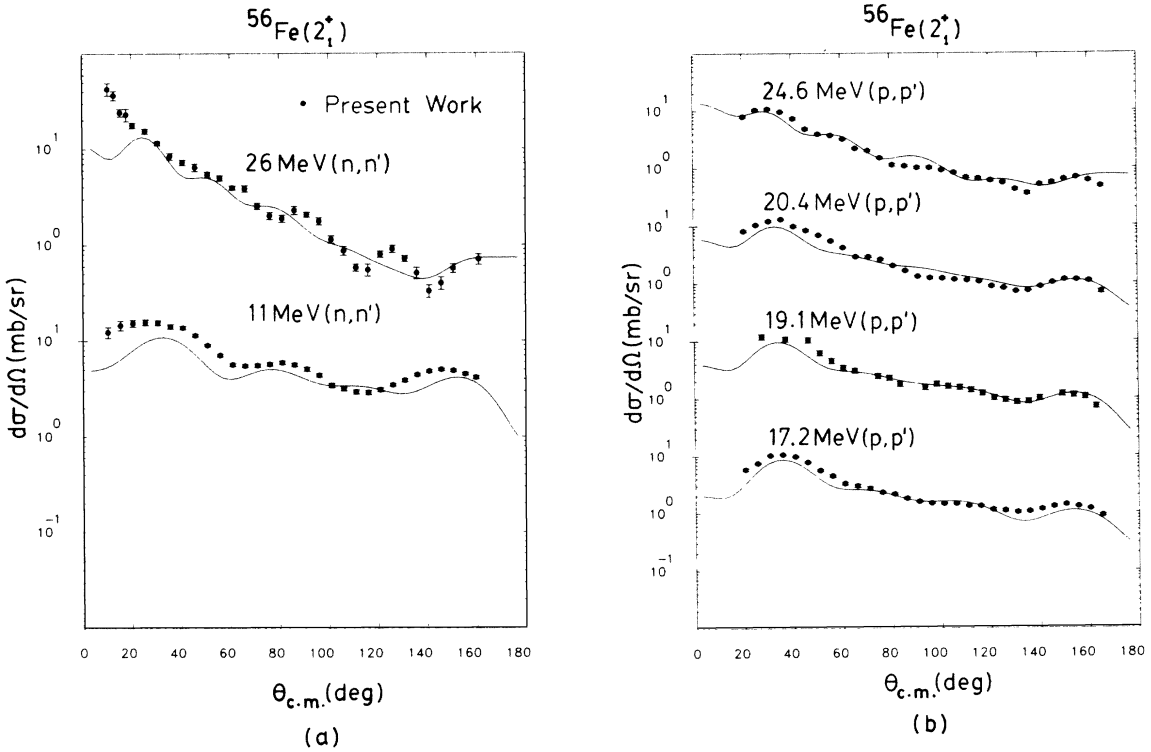

FIG. 11. Microscopic DWBA calculations of scattering to the 2_1^+ state ($E_x=0.85$ MeV) in ^{56}Fe are compared to (a) the neutron data of the present work and (b) proton data from the literature. The 19.1 MeV data are from Ref. 6 and the remaining data are from Ref. 9.

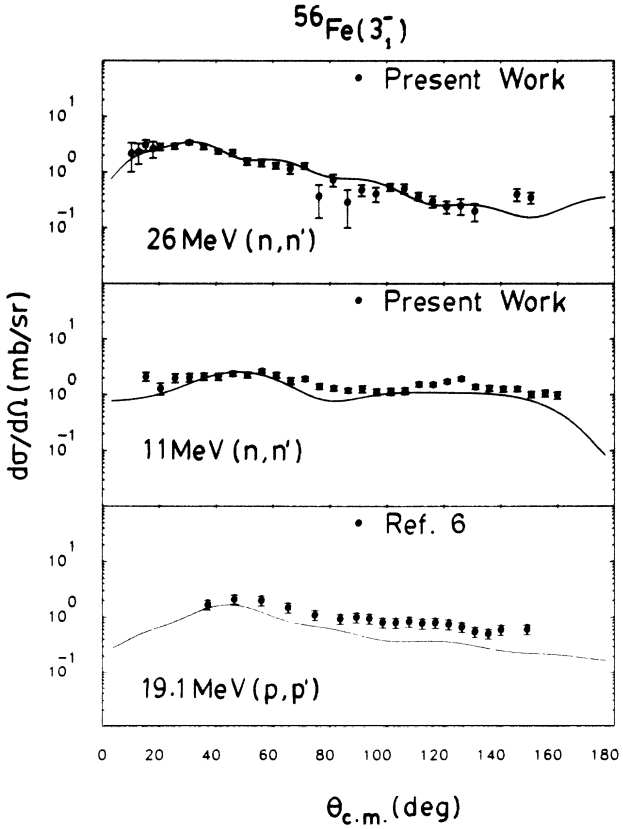

FIG. 12. Microscopic DWBA calculations of scattering to the 3_1^- state ($E_x=4.51$ MeV) in ^{56}Fe are compared to the neutron data of the present work and the proton data of Ref. 6.

present work shows that further investigations of the quality of the effective interaction, the adequacy of the exchange approximation, and the influence of the distorting potential will be required.

IV. NEUTRON-PROTON COMPARISON

The isospin character of a particular excitation may be investigated by comparing neutron and proton inelastic scattering measurements. A quantitative description of the isospin nature of an excitation is usually expressed as M_n/M_p, the ratio of neutron and proton transition matrix elements, which are defined by

$$M_{n(p)} \equiv \int \rho_{tr}^{n(p)}(r) r^{\lambda+2} dr \tag{4}$$

for a transition of multipolarity λ.

The deformation parameters $\beta_{nn'}$ and $\beta_{pp'}$ extracted from DWBA analysis (or, more properly, the deformation lengths $\delta_{nn'}=R\beta_{nn'}$ and $\delta_{pp'}=R\beta_{pp'}$, where R is the radius of the optical potential) may be used[3] to calculate M_n/M_p. In the limit that $\delta_{nn'}=\delta_{pp'}$, the quantity $M_n/M_p=N/Z$.

Table VI is a summary of the values available in the literature for $\beta_{pp'}$ for low-lying excitations in ^{54,56}Fe. Most of the weakly excited 2^+ and 4^+ states have only been measured at one energy (49.4 MeV) by Mani.[7,8] However, Mani's values of $\beta_{pp'}$ are 20–50% lower than those obtained in more recent measurements of the strongly excited states. This casts doubt upon the reliability of Mani's data in a proton-neutron comparison, and makes it impossible to perform such a comparison for any of the weakly excited 2^+ and 4^+ states. We recall that

TABLE VI. Deformation parameters from the literature for DWBA analysis of ^{54,56}Fe(p,p').

Nucleus	State	Incident energy (MeV)	$\beta_{pp'}$	r_R
^{54}Fe	2_1^+ (1.41 MeV)	17.2	0.15 ±0.01	1.15[a]
		18.6	0.16 ±0.01	1.25[b]
		20.4	0.16 ±0.01	1.15[a]
		24.6	0.15 ±0.01	1.15[a]
		35.2	0.16 ±0.01	1.16[c]
		49.4	0.130±0.013	1.20[d]
	4_1^+ (2.55 MeV)	49.4	0.050±0.005	1.20[d]
	2_2^+ (2.96 MeV)	17.2	0.14 ±0.01	1.15[a]
		20.4	0.13 ±0.01	1.15[a]
		24.6	0.13 ±0.01	1.15[a]
		49.4	0.098±0.010	1.20[d]
	2_3^+ (3.17 MeV)	49.4	0.047±0.005	1.20[d]
	4_2^+ (3.30 MeV)	49.4	0.033±0.003	1.20[d]
	4_3^+ (3.83 MeV)	49.4	0.052±0.005	1.20[d]
	4_4^+ (4.05 MeV)	49.4	0.024±0.002	1.20[d]
	4_5^+ (4.27 MeV)	49.4	0.045±0.005	1.20[d]
	3_1^- (4.78 MeV)	18.6	0.13 ±0.01	1.25[b]
		49.4	0.069±0.007	1.20[d]
	3_2^- (6.40 MeV)	18.6	0.16 ±0.01	1.25[b]
^{56}Fe	2_1^+ (0.85 MeV)	17.2	0.26 ±0.01	1.15[a]
		19.1	0.28 ±0.03	1.25[b]
		20.4	0.26 ±0.01	1.15[a]
		24.6	0.24 ±0.01	1.15[a]
		35.2	0.245±0.025	1.16[a]
		49.4	0.20 ±0.01	1.20[e]
	2_2^+ (2.66 MeV)	49.4	0.06 ±0.01	1.20[e]
	2_3^+ (2.96 MeV)	49.4	0.02 ±0.01	1.20[e]
	4_2^+ (3.12 MeV)	49.4	0.087±0.009	1.20[e]
	2_4^+ (3.37 MeV)	49.4	0.06 ±0.01	1.20[e]
	2_5^+ (3.60 MeV)	49.4	0.05 ±0.01	1.20[e]
	2_6^+ (3.83 MeV)	49.4	0.03 ±0.01	1.20[e]
	4_3^+ (4.12 MeV)	49.4	0.045±0.005	1.20[e]
	3_1^- (4.51 MeV)	19.1	0.20 ±0.04	1.25[b]
		49.4	0.154±0.15	1.20[e]

[a]Reference 9.
[b]Reference 6.
[c]Reference 10.
[d]Reference 7.
[e]Reference 8.

the parameters $\beta_{nn'}$ extracted from the present 11 MeV analysis for both ^{54,56}Fe(n,n') are consistently less than the corresponding values obtained in the 26 MeV analysis. This was attributed to an overestimate of the compound nuclear contribution to our measured cross sections at 11 MeV. For ^{54}Fe we are left, then, with a comparison between the values of $\beta_{nn'}$ from the present 26 MeV analysis and the values of $\beta_{pp'}$ from the literature (excluding those at 49.4 MeV) for the 2_1^+, 2_2^+, and 3_1^- states. For the latter two states it can be seen that $\delta_{nn'} \approx \delta_{pp'}$. For the first 2^+ state, on the other hand, clearly $\delta_{nn'} > \delta_{pp'}$. Using the values $\delta_{nn'} = 0.868 \pm 0.09$ from the 26 MeV analysis and $\delta_{pp'} = 0.62 \pm 0.02$ from the average of the literature values, one may calculate $M_n / M_p = 0.78 \pm 0.07$. While the absolute value of this number is somewhat uncertain (since the values of $\delta_{nn'}$ and $\delta_{pp'}$ come from totally separate analy-

ses), it is a manifestation of the closed neutron shell in ^{54}Fe, which suppresses the neutron contribution to the first 2^+ transition. For ^{56}Fe, comparison of the values of $\delta_{nn'}$ and $\delta_{pp'}$ for both the 2_1^+ and 3_1^- excitation in ^{56}Fe seems to indicate that $\delta_{nn'} \approx \delta_{pp'}$ in both cases.

To investigate whether channel coupling modifies the values of M_n/M_p obtained above, the coupled-channels analysis described in Sec. III was extended to the proton-scattering data of Van Hall *et al.*[9] for ^{54,56}Fe at 17.2, 20.4, and 24.6 MeV. For ^{54}Fe, the phonon-mixing vibrational model yielded an average value of $\delta_{pp'}=0.865\pm0.04$ compared to the value $\delta_{nn'}=0.953\pm0.05$ from the 26 MeV analysis. This results in the value $M_n/M_p=0.89\pm0.06$ for the 2_1^+ excitation, which is slightly larger than the value obtained in DWBA, but consistent with it. For ^{56}Fe, the rotational model applied to the proton data led to the conclusion that $\beta_{pp'}=\beta_{nn'}=0.245\pm0.005$, confirming the conclusion that $M_n/M_p \approx N/Z$ for this excitation.

As pointed out in Sec. III, the density-dependent folding model analysis of scattering to the 2^+ and 3^- states measured at 26 MeV was consistent with the value $M_n/M_p=N/Z$ for all except the first 2^+ excitation in ^{54}Fe, where $M_n/M_p=0.8\pm0.1$.[25]

The work of Brown and Madsen[1-3] on singly-closed-shell nuclei predicts that $\beta_{nn'}>\beta_{pp'}$ for a closed neutron-shell nucleus, and their one-parameter schematic core polarization model yields a value[32] of $M_n/M_p=0.844$ for the 2_1^+ state in ^{54}Fe, which is significantly different from the collective model value $M_n/M_p=N/Z=1.08$. At the same time, a recent extension of their model to open-shell nuclei predicts that the strong isovector effects at shell closure disappear rapidly with the addition of a few nucleons outside the closed shell.[33] The present analysis is in agreement with these predictions.

V. SUMMARY

The inelastic neutron scattering data measured with the Ohio University beam-swinger time-of-flight facility on ^{54,56}Fe are of sufficient quality to allow a search for proton-neutron transition density differences to several excited states by comparison with proton scattering. The analysis has been carried out in a microscopic DWBA approach, in which the neutron and proton transition densities are a direct input to the calculations, and also in a conventional DWBA model in which the transition form factor is related to the deformation of the optical potential. Coupled-channel calculations were also performed for the conventional model.

The microscopic folding model DWBA analysis using the Brieva-Rook interaction reproduces the angular-distribution shapes and magnitude of 2^+ excitations quite well, with transition densities that are consistent with electron-scattering and Coulomb-excitation results. The shapes of 3^- angular distributions are given correctly, but the magnitudes predicted with transition densities normalized to electromagnetic results are lower than the data by roughly 30%.

Both the collective and microscopic model comparisons of neutron and proton scattering are in agreement that the 2_1^+ excitation in ^{54}Fe is dramatically affected by shell closure, and that $\beta_{nn'}>\beta_{pp'}$ (i.e., that $M_n/M_p<N/Z$). Both analyses are also in agreement that such a shell-closure effect is not in evidence for several higher excited states in ^{54}Fe. Furthermore, shell-closure effects are not observed for either the 2_1^+ or 3_1^- states in ^{56}Fe, where only two neutrons are present outside the closed shell.

The present analysis is in agreement with the core polarization models of Brown and Madsen[1-3] and, as far as the 2_1^+ states in ^{54,56}Fe are concerned, is also in agreement with the lower energy neutron scattering analysis of Delaroche *et al.*[13] However, our conclusion that the 2_1^+ excitation in ^{56}Fe does not exhibit an isovector component in the deformation parameter disagrees with the conclusions of Orihara *et al.*[34] and Maeda.[35] Their analysis of ^{56}Fe(p,n)^{56}Co to the excited analog 2^+ state concludes that $\beta_1/\beta_0 \sim 3$ for this excitation. On the other hand, the present work, and in particular the consistent coupled-channels analysis in which the same deformation parameter can be used to describe both proton and neutron scattering to this state, implies that $\beta_1/\beta_0=1$. One possible source of this disagreement may be that, while it is demonstrated in Ref. 34 that two-step processes in the coupled-channels formalism are essential in reproducing the measured (p,n) cross sections, such processes were ignored in their extraction of the isovector deformation parameter β_1. As pointed out by Madsen and Brown,[36] such an extraction of β_1 is impractical because the amplitudes for the two-step mechanisms are both large and out of phase with the direct term.

The present analysis has shown that while a coupled-channel analysis describes the data well, the main features of the data are adequately described by the DWBA. Channel-coupling effects on the shapes of the angular distributions are subtle, and the deformation parameters are only slightly altered from their DWBA values.

Finally, there is one glaring disagreement between the measured neutron scattering data and all the various forms of analysis. The sharp rise in the forward angle measurements of the 2_1^+ cross sections for both ^{54,56}Fe at 26 MeV is not reproduced by either the collective-model or the microscopic-model analysis. We are confident that the measurements are correct, and that the cross sections do indeed exhibit the indicated behavior. The inelastic cross sections were extracted using a simultaneous peak-fitting procedure in which all peaks in a given spectrum were assumed to have the same shape as the elastic peak. The absence of background and the quality of the resolution of the first 2^+ state from the ground state at 25 MeV may be seen in Fig. 2. While this spectrum was taken at a lab angle of 35°, the resolution at more forward angles was only slightly worse. In every case the peak of the first 2^+ excitation was clearly visible in the spectrum, and any uncertainties introduced by peak fitting are included in the error bars shown. The possibility of elastic multiple scattering contaminating the region of the 2^+ peak was eliminated by performing Monte Carlo calculations of TOF spectra for the given experimental conditions. These calculations allowed for downscattering of the neutron energies. The calculations showed no effect in the region of the 2^+ peak, but did affect the low-energy tail of the elas-

tic peak shape as expected. It should also be noted that unexpectedly large forward-angle, first-excited-state cross sections at $E_n > 20$ MeV are not limited to the cases of ^{54,56}Fe. Recent measurements[37] of the first 3^- state in ^{208}Pb at $E_n = 20$ and 22 MeV exhibit the same behavior. In that case the large excitation energy (2.625 MeV) precludes any questions of resolution or elastic contamination.

Comparison with other measurements to the states in ^{54,56}Fe is impossible, as no other data exist for either (n,n') or (p,p') at lab angles less than 20°. One possible explanation is that all of our calculations treat the nonlocality of knockout exchange in a zero-range approximation. It would be interesting to see whether a calculation with a model wave function and an exact treatment of exchange could resolve this discrepancy.

ACKNOWLEDGMENT

This work was performed under the auspices of the National Science Foundation under Grant No. PHY-8108456 and the Department of Energy by the Lawrence Livermore National Laboratory under Contract No. W-7405-ENG-48.

---

*Present address: Physics Department, University of Wisconsin—Madison, Madison, WI 53706.

[1]V. R. Brown and V. A. Madsen, Phys. Rev. C **11**, 1298 (1975).
[2]V. A. Madsen, V. R. Brown, and J. D. Anderson, Phys. Rev. C **12**, 1205 (1975).
[3]A. M. Bernstein, V. R. Brown, and V. A. Madsen, Phys. Lett. **103B**, 255 (1981).
[4]D. E. Bainum *et al.*, Nucl. Phys. **A311**, 492 (1978).
[5]R. W. Finlay *et al.*, Nucl. Phys. **A338**, 45 (1980).
[6]S. F. Eccles, H. F. Lutz, and V. A. Madsen, Phys. Rev. **141**, 1067 (1966).
[7]G. S. Mani, Nucl. Phys. **A157**, 471 (1970).
[8]G. S. Mani, Nucl. Phys. **A165**, 225 (1971).
[9]P. J. Van Hall *et al.*, Nucl. Phys. **A291**, 63 (1977).
[10]E. Fabrici *et al.*, Phys. Rev. C **21**, 844 (1980).
[11]P. Boschung, J. T. Lindow, and E. F. Shrader, Nucl. Phys. **A161**, 593 (1971).
[12]S. M. El-Kadi *et al.*, Nucl. Phys. **A390**, 509 (1982).
[13]J. P. Delaroche *et al.*, Nucl. Phys. **A390**, 541 (1982).
[14]R. W. Finlay *et al.*, Nucl. Instrum. Methods **198**, 197 (1982).
[15]S. Mellema, R. W. Finlay, F. S. Dietrich, and F. Petrovich, Phys. Rev. C **28**, 2267 (1983).
[16]W. E. Kinney, Oak Ridge National Laboratory Report ORNL-TM-2052, 1968.
[17]E. D. Arthur and P. G. Young, Los Alamos Scientific Laboratory Report LA-8626-MS, 1980.
[18]S. K. Penney, Oak Ridge National Laboratory Report ORNL-TM-2590, 1969.
[19]P. D. Kunz, private communication.
[20]J. Raynal (unpublished).
[21]D. G. Sarantites, J. Urbon, and L. L. Rutledge, Phys. Rev. C **14**, 1412 (1976).
[22]J. B. McGrory and S. Raman, Phys. Rev. C **20**, 830 (1979).
[23]M. J. Levine, E. K. Warburton, and D. Schwalm, Phys. Rev. C **23**, 244 (1981).
[24]A. S. Meigooni, R. W. Finlay, J. S. Petler, and J. P. Delaroche, Nucl. Phys. (in press); A. S. Meigooni, Ph.D. dissertation, Ohio University, 1984.
[25]S. Mellema, R. W. Finlay, F. S. Dietrich, and F. Petrovich, Phys. Rev. C **29**, 2385 (1984).
[26]F. A. Brieva and J. R. Rook, Nucl. Phys. **A291**, 299 (1977).
[27]F. A. Brieva and J. R. Rook, Nucl. Phys. **A291**, 317 (1977).
[28]J. Bellicard and P. Barreau, Nucl. Phys. **36**, 476 (1962).
[29]J. M. Moss, D. L. Hendrie, C. Glashausser, and J. Thirion, Nucl. Phys. **A194**, 12 (1972).
[30]R. J. Peterson, H. Theissen, and W. J. Alston, Nucl. Phys. **A153**, 1610 (1970).
[31]F. S. Dietrich and F. Petrovich, in *Neutron-Nucleus Collisions—A Probe of Nuclear Structure*, Proceedings of the Conference on Neutron-Nucleus Collisions—A Probe of Nuclear Structure held in Burr Oak State Park, Glouster, Ohio, 1984, AIP Conf. Proc. No. 124, edited by J. Rapaport, R. W. Finlay, S. M. Grimes, and F. S. Dietrich (AIP, New York, 1985), p. 90.
[32]V. A. Madsen, private communication.
[33]V. A. Madsen and V. R. Brown, Phys. Rev. Lett. **52**, 176 (1984).
[34]H. Orihara *et al.*, Phys. Lett. **106B**, 171 (1981).
[35]K. Maeda *et al.*, Nucl. Phys. **A403**, 1 (1983).
[36]V. A. Madsen and V. R. Brown, in *The (p,n) Reaction and the Nucleon-Nucleon Force*, edited by C. Goodman *et al.* (Plenum, New York, 1980), p. 461.
[37]R. W. Finlay *et al.*, Phys. Rev. C **30**, 796 (1984).